Pergamon

PII: S0191–8141(97)00113–2

Journal of Structural Geology, Vol. 20, No. 5, pp. 529 to 548, 1998

0191-8141/98 $19.00 + 0.00

The geometry of polygonal fault systems in Tertiary mudrocks of the North Sea

LIDIA LONERGAN, JOE CARTWRIGHT and RICHARD JOLLY

Department of Geology, Imperial College, London, SW7 2BP, U.K. (l.lonergan@ic.ac.uk)

(*Received* 23 *May* 1997; *accepted in revised form* 11 *November* 1997)

Abstract—Polygonal networks of extensional faults have recently been identified deforming large volumes of Tertiary mudrocks in the North Sea. The main distinctive feature of this fault system is a near equal distribution of fault strike orientations and polygonal organisation of the fault trace segments in plan view. Detailed fault mapping using three-dimensional seismic reflection datasets from the central North Sea show that the complex three-dimensional geometries are primarily a function of intersections between fault surfaces oriented in all directions in space. Within stratigraphic units or layers the deformation is distributed as opposed to the clustered deformation of more co-linear tectonic fault arrays where the strain is concentrated into zones or bands at a variety of scales. End member map patterns with curved, rectilinear or irregular polygonal geometries are identified that encompass the variability observed on over 30 fault maps made at different stratigraphic levels within the three-dimesional seismic datasets.

Four main classes of intersections between fault segments are defined providing a descriptive geometric framework for polygonal fault systems. The geometry of the intersection types and their geometrical stability in three-dimensions is discussed with reference to examples from the seismic datasets.

Fault shapes are irregular and, in detail, shape is largely a function of intersection relationships with neighbouring faults. Faults can be planar or listric, and can have triangular shapes that may taper upwards or downwards. They frequently exhibit complex irregular upper tips. Completely isolated non-connected faults are very rare within the three-dimensional datasets studied.

INTRODUCTION

Recently a new type of fault system developed in Tertiary sediments in the North Sea has been described based on the analysis of seismic datasets (Cartwright, 1994a,b; Cartwright and Lonergan, 1996; Cartwright, 1996). The distinctive feature of these faults is that in plan view they are polygonally organised with no regionally consistent preferred strike orientation. The faults have exclusively normal displacements with average throws of around 30–50 m (Lonergan *et al.*, 1998; Lonergan and Cartwright, in press). Typical fault trace lengths range from 100 m–1000 m. The polygonal fault system is organised in stratigraphically defined layers, with the deformation apparently being decoupled between the layers. Each layer or tier has a different spacing and orientation of faults (Cartwright, 1994b, 1996). Using a regionally extensive two-dimensional seismic dataset Cartwright, (1994a,b) identified two main tiers of faults related to the gross sequence stratigraphy in the North Sea. Subsequent analyses of three-dimensional datasets have suggested that there can be up to three or more sets of polygonal faults stacked vertically in anyone area (Cartwright; 1996, Lonergan and Cartwright, in press).

Within the North Sea the faults are restricted to Paleocene–Lower Miocene mudrock dominated sequences of the slope and basin floor depositional systems (Fig. 1a) and Cartwright and Lonergan (1996) have suggested that the polygonal faults have formed in response to three-dimensional compaction of the fine-grained sediments during early burial. The polygonal faults exhibit radial strain patterns in plan view with approximately 20% apparent areal extension within any one layer. Since the deformation is layer bound and there is no evidence of extensional displacement transfer onto basement structures in the North Sea, Cartwright and Lonergan (1996) argue that the only explanation for the apparent extension is for layer-parallel volumetric contraction to have occurred. Part of the volume reduction due to pore fluid loss is thus accommodated by extensional faulting.

This basin-scale deformation structure is not restricted to the North Sea Basin alone. Polygonal faults have now been described and identified in the Eromanga basin of Australia (Oldham and Gibbins, 1995; Cartwright and Lonergan, 1997) and Cartwright and Dewhurst (in press) have interpreted similar layer-bound extensional faults within fine-grained sedimentary sequences in at least another 26 basins around the world.

The polygonal fault systems can be considered an end-member in a range of natural faulting styles. In contrast to faults forming in response to a tectonic event, the polygonal faults have no systematic strike distributions, and represent one of the most interconnected meso-scale fault sets documented to date. Of naturally occurring fracture systems, joints sets are also highly connected, but tend to have simpler and more regular geometries (e.g. Pollard and Aydin, 1988). Although the density, spacing and pattern of

the polygonal faults vary in different areas in the North Sea on a kilometre-scale there are approximately equal numbers of faults in any direction forming a distributed deformation. This is distinctly different to the clustering of fault arrays that are observed at a range of scales typical of tectonic deformation (e.g. Cowie *et al.*, 1993).

In this paper we systematically describe the three-dimensional geometry, including intersection relationships of this new class of faults. In the first part of the paper we describe the variety of fault patterns expressed on maps. The spatial pattern of a fault or fracture system results from the interplay of several attributes. To uniquely characterise two-dimensional fault patterns, descriptions of attributes such as fault orientations, size distributions, linkage, density or spacing and fault trace shapes are required (Gillespie *et al.*, 1993). Although some of these parameters are easily measured (e.g. orientation and length distributions) others, such as spacing and linkage are much more difficult to quantify especially in two or three dimensions. We document the main features and variability of the polygonal fault maps by examining fault trace orientations, fault length distributions, fault intersection angles, fault trace shape and fault density. In the second part of the paper we discuss the main three-dimensional intersection types that occur between intersecting fault segments and conclude that the geometry of the complex intersecting array of fault segments is primarily a function of intersections between faults that propagated in all directions during their growth.

Datasets and methodology

Data from six three-dimensional reflection seismic surveys located within the central North Sea (Fig. 1a) have been used for the fault analysis. These datasets are high-resolution with line and trace spacings being either 12.5 m or *ca.* 25 m. In the best imaged parts of

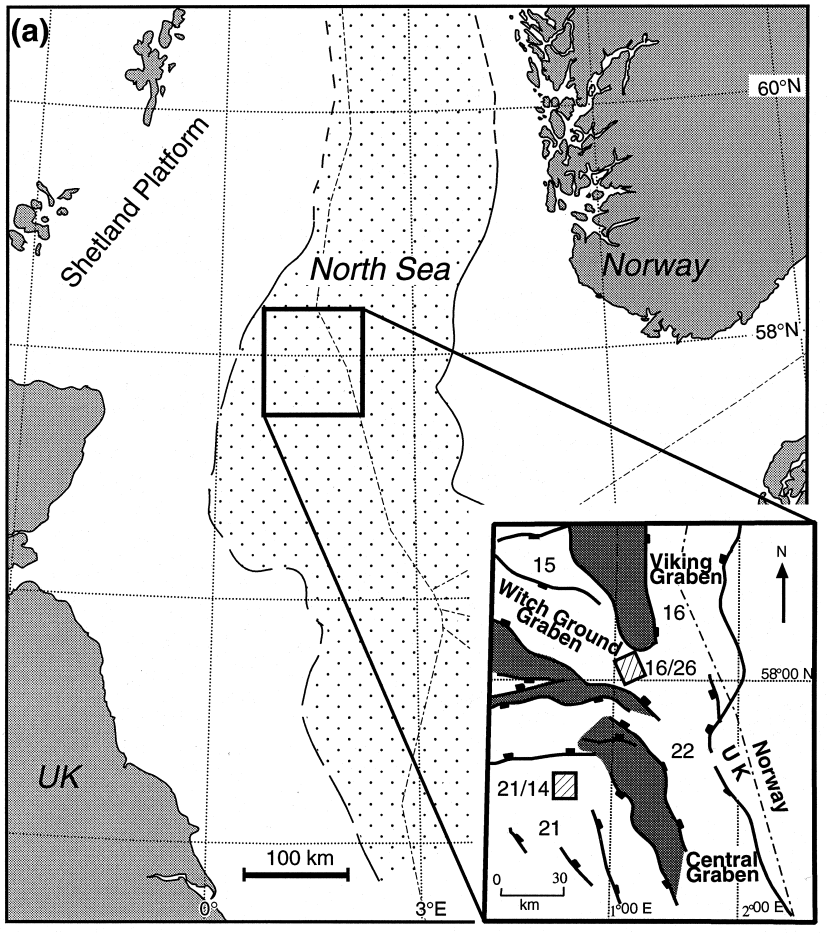

Fig. 1(a).

the surveys, with strong amplitude reflections, faults with displacements as small as 4 ms two-way travel time (TWT) (i.e. approximately 4 m, at a velocity of 2000 m/s) can be resolved. Although offsets on seismic reflections clearly indicate the presence of faults on vertical seismic sections, the complexity of the deformation means that on any one vertical section it is very difficult to make a unique fault interpretation (Fig. 1b; see Cartwright, 1996 for more detail). In contrast maps of stratigraphic markers offset by faults provide a very clear plan view of the fault geometry (Fig. 1c). Horizon maps are made by interpreting a stratigraphic marker with a strong seismic response throughout the seismic volume. Offsets on the seismic event or marker are projected as fault heave onto the map. Fault maps generated in this way are the the best dataset that can be extracted from the seismic volume. The area covered by a single three-dimensional survey is typically greater than about 36 km^2.

Recent advances in data processing allow the three-dimensional seismic volume to be processed for coherency or cross-correlation between a seismic trace and its surrounding neighbouring traces (Bahorich and Farmer, 1995). Faults offset the seismic signal between traces and hence are regions of low coherence or correlation. When a correlation process is applied to a time window of seismic data centred around a marker horizon fault trace maps can be generated automatically. Compare Fig. 1(c) where the fault map was made by interpreting every line in the survey (a few weeks work) with Fig. 1(d) which is the result of processing the seismic data in the same interval for cross-correlation (a few minutes processing time on a workstation). This result confirms that the fault maps are not interpreter-dependent and are a true representation, within resolution of the seismic reflection imaging technique, of the deformation in plan-view in the dataset.

Fault interpretation is achieved by using a series of closely spaced maps to guide the interpretation. This helps avoid any spatial aliasing. The faults are interpreted on vertical sections selected in an orthogonal orientation to the fault strike on the map, and on the maps themselves. A fault surface is then constructed by triangulating the interpreted points that have been assigned to the fault. Given the highly inter-connected nature of the polygonal fault system, fault interpretation proceeds iteratively until a geometrically and structurally consistent three-dimensional geometry is obtained.

Fault nomenclature and sources of error

A single slip surface is easily identified as a fault when it is isolated in space and defined by a continuous, closed tip-line (Barnett *et al.,* 1987; Gillespie *et al.*, 1992). In practice faults are rarely isolated and when faults are connected wholly or partially with other faults it is not always immediately apparent from

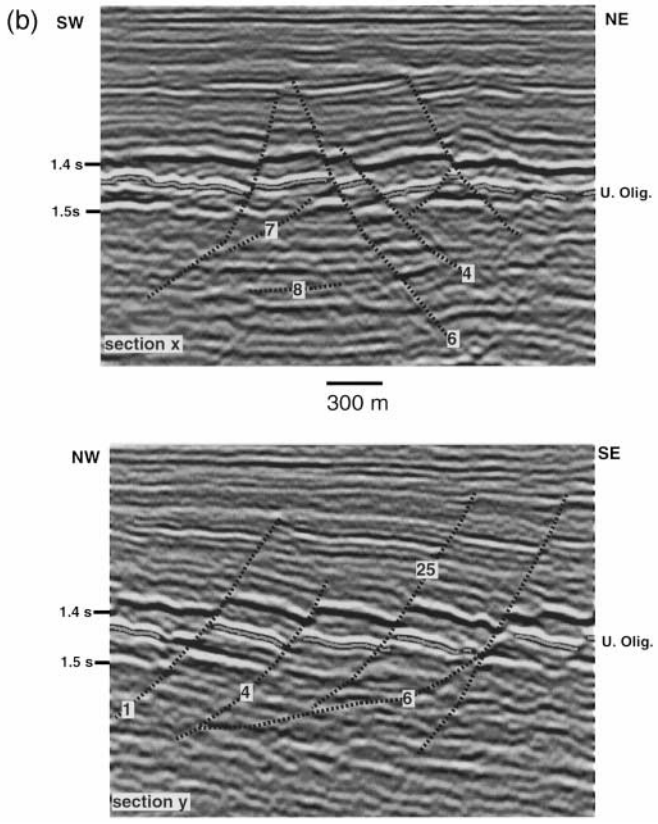

Fig. 1(b).

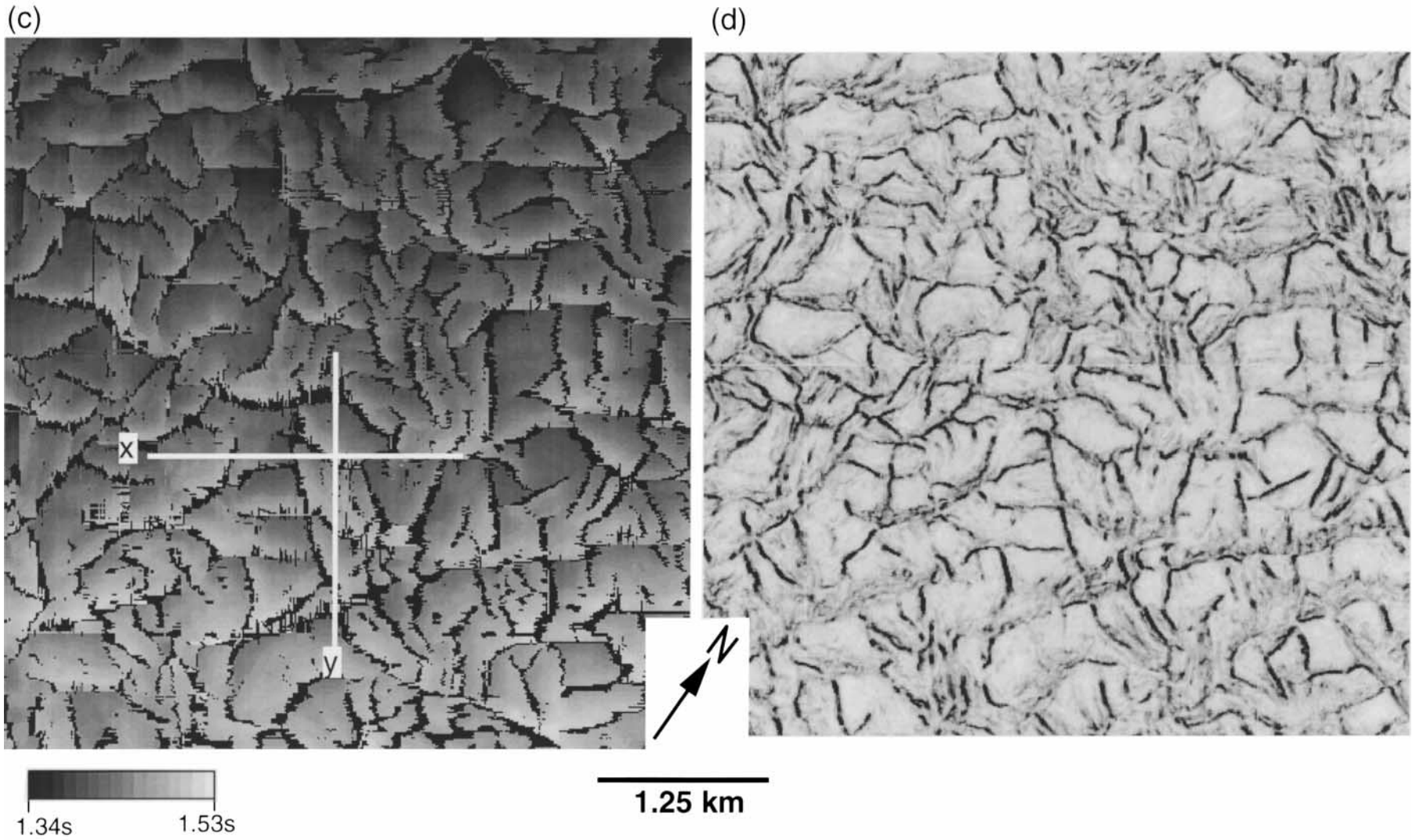

Fig. 1. (a) Distribution of polygonal faults in the North Sea. Inset map shows main Mesozoic tectonic features of the Central North Sea, quadrant names and location of seismic datasets discussed in text. (b) Seismic sections from a three-dimensional dataset in block 16/26. The two lines are mutually orthogonal. The grey interpreted horizon is Upper Oligocene in age. Location of lines are shown in the map in (c). Some of the interpreted faults (dotted black line), and those labelled, are discussed in the text and illustrated in Fig. 9. Vertical scale is seconds, two-way travel time. (c) Horizon map of an Upper Oligocene horizon in the block 16/26 dataset, contoured in two-way-travel time. The gaps in the horizon (black) and offsets of time-contours are caused by faulting. (d) Attribute map of coherence (Geoquest–Charisma correlation function) calculated in an 80 ms time window, containing the high amplitude peak of the Upper Oligocene marker horizon, centered around a timeslice at 1450 ms. The black–dark grey shades are regions of low correlation between neighbouring seismic traces and are interpreted as faults. Note the correspondence between the fault map pattern in (c) and the fault pattern on the correlation attribute map calculated without any prior user interpretation.

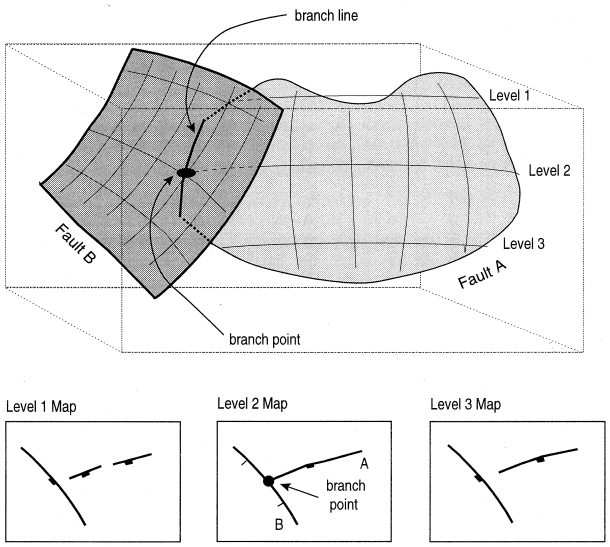

Fig. 2. Faults A and B intersect at a branch line, but the branch line does not divide Fault B into two segments along its entire height; Fault A has an irregular upper tip. Maps made at different vertical levels may not give a 'true' representation of the three-dimensional geometry.

either maps or vertical sections which fault trace segments belong to a single fault surface. In general, connected fault trace segments of the same strike on a map (Fig. 2, level 2 map) are likely to form a continuous fault surface when mapped in three-dimensions, although such a segmented fault may have originated by the linkage of a number of initially separate segments (Peacock and Sanderson, 1991; Dawers *et al.*, 1993; Cartwright *et al.*, 1995). The identification of what constitutes a single fault also depends on the scale of the observation (Gillespie *et al.*, 1992). A fault trace represented by a single line on a map may be seen to consist of several trace segments when viewed on a larger scale map.

A branch line is defined as an intersection between two or more fault surfaces (e.g. Diegel, 1986) and can be considered to be made up of a series of branch points. Thus the intersection of a branch line with an observation plane (e.g. map or section) is a branch point, and is referred to as such in this paper (Fig. 2). If the intersection of two or more fault segments occurs at a single geometrical position then the intersection will be a branch point as opposed to a branch line.

A branch line need not be continuous and segment a fault plane into two separate surfaces along its entire height (Fig. 2). For example Fault B in Fig. 2 has two fault trace segments on a map made at level 2, but only one trace segment at maps made at levels 1 and 3. Two aligned fault traces of the same strike, but not connected on a map, may be found to belong to a single fault surface which has an irregular upper tip geometry (Fault A in Fig. 2, map level 1), or to join at depth to a single fault at either a branch line or branch point (e.g. fig. 2, Childs *et al.,* 1995). Without *a priori* knowledge of the three-dimensional fault geometry, using maps and sections it can be impossible to make consistent interpretations of which fault trace segments belong to a single fault. Although ideally we would like to map all faults in three-dimensions this is not feasible, and the limitations of working with plan or section data have to be accepted.

We use the terms 'branch line' and 'branch point' in a purely geometrical sense (e.g. Diegel, 1986). In the use of the term branch line/point we are not implying that a 'parent' fault branched into two or more segments as opposed to the opposite case where two or more initially independent fault segments merged during growth (cf. Willemse, 1997).

In this study, fault population statistics (e.g. length and orientation) have been recorded on map data for each fault trace segment. Where a continuous fault trace of the same strike is segmented (e.g. Fig. 2, Fault B, map level 2) we record it as a single fault trace. Curved fault surfaces are common on some data sets and though the strike changes it does so in a smooth and regular manner and curved fault segments are interpreted as a single fault. On maps the strike of curved fault traces is approximated as the orientation of a line drawn between the two endpoints (either a free tip or an intersection), which is close to the mean strike of the fault. The length is measured along the curved trace.

The interpretation of faults on seismic datasets is affected by the resolution limit of the method (Sheriff, 1977). The limit of seismically resolvable displacement determines the position of an apparent fault tip. We have to assume that the the overall fault segment shape is similar to the mapped apparent fault tip or intersection termination. This approximation seems reasonable, particularly for the better quality datasets where the displacement resolution is of the order of 4 m.

Similarly any fault population statistics extracted from map data will also be subject to this resolution limit error (see Heffer and Bevan, 1990 and Pickering *et al.,* 1997 for a fuller discussion of other sampling and censoring errors associated with fault population statistics). In particular the lengths of fault trace segments will be underestimated because of the restriction on the minimum throw that can be seen (Pickering *et al.*, 1997). Fault trace segments that terminate at an intersection that is above the resolution limit will not be subject to this error. We attempt to minimise these errors by using seismic attribute maps such as dip, azimuth, and edge detection techniques, (Dalley *et al.*, 1989; Hoetz and Watters, 1992) to extend the range of faults that we image. These attributes can be used to identify faults close to the seismic resolution that may only perturb a reflection as opposed to offsetting it.

GEOMETRICAL CHARACTERISTICS OF POLYGONAL FAULT SYSTEMS IN PLAN VIEW

In general the common characteristic of all maps of the extensional fault system developed in mudrocks of the North Sea is that the faults are organised in a superficially polygonal pattern (Cartwright, 1994a,b; Cartwright and Lonergan, 1996; Cartwright, 1996). The map patterns resemble the polygonal networks of cracks and fractures that occur at a variety of scales in natural media which undergo a volume change (e.g. cracks in ceramic glazes and concrete, desiccation cracks in muds and playa lakes, ice-wedge polygons in frozen ground, columnar joints in lavas; Kindle, 1917; Lachenbruch, 1962; Neal *et al.*, 1968; Plummer and Gostin, 1981; Allen, 1987; Korvin, 1992). The fault patterns are not entirely polygonal because not all the faults connect to define closed cells in plan view. Some of the maps have fault patterns that resemble the incomplete stage of desiccation in muds where not all the cracks have connected to make closed polygons (see the experiments of Corte and Higashi, 1964; or natural examples in Plummer and Gostin, 1981; Allen, 1987). However 'polygonal' still seems to be the best approximation of a plan view geometry where planar, curved and sinuous fault traces are distributed in a wide variety of orientations and connect to form both closed and open multi-sided cells.

Fault trace patterns

A variety of fault map styles have been identified from the mapping of over 30 stratigraphic horizons within six different three-dimensional seismic surveys in the central North Sea. Based on fault trace orientation, intersection angle, spacing, and fault trace linkage or connectivity these can be divided into four main types as follows (Fig. 3):

(a) A regular-rectangular polygonal pattern, where the majority of intersection angles are orthogonal (Fig. 3a).
(b) A curved polygonal pattern dominated by curved fault traces with a broad spread of intersection angles, between 90° and 140° (Fig. 3b).
(c) An irregular, well-connected polygonal pattern, with linear and curved fault traces and a predominance of orthogonal intersection angles (Fig. 3c).
(d) An irregular, poorly-connected fault pattern with short fault traces, which tend to be grouped or aligned in clusters (Fig. 3d).

The regular-near-rectangular (Fig. 3a) and curved (Fig. 3b) patterns can be considered to be two end-member geometries, with the irregular pattern (Fig. 3c) representing an intermediate form. With the analysis of more datasets, the fourth type described (Fig. 3d) may prove to be another variant of an intermediate type. In the meantime it is considered sufficiently distinct to warrant identifying it separately. Poorer connectivity is not just restricted to this fault pattern type. This suggests that connectivity may be a property that reflects the 'maturity' of the fault network, with low connectivity patterns forming where the faults have not continued to grow and link up to form a highly connected network. In some cases the lack of connectivity may only be *apparent* and occur as a function of the fault dimension and data resolution and/or quality. If the faults are smaller and more closely spaced forming at a scale close to the data resolution then only the larger faults will be imaged and the smaller connecting fault segments may not be imaged. Similarly in areas of poorer data quality the resultant interpretation will yield apparently less well-connected fault networks.

On the datasets examined thus far, the most common geometry is a variant of the irregular polygonal pattern (Fig. 3c). We have also observed that at any given stratigraphic level, the fault pattern can change type and dimension (i.e. both average fault segment length and spacing/density) over distances of a few kilometres. Also vertically in any one dataset the map pattern can change dramatically between different stratigraphic levels (see for example Cartwright, 1996; Lonergan and Cartwright, in press) which comprise distinct faulted layers or tiers (compare the maps in Fig. 4a,b & d, which come from the same data set, but at different vertical stratigraphic levels).

Type examples of each of these fault map styles are illustrated in Fig. 4. The maps were made at a number of different stratigraphic intervals spanning the Eocene–Lower Miocene from two different seismic surveys in quadrants 21 and 16 of the central North Sea (Fig. 1a). Irrespective of the polygonal pattern type, fault trace segments are distributed in a wide variety of orientations with approximately equal numbers of faults in all directions (Fig. 5a). Local biases in fault segment orientations do occur. These biases sometimes reflect underlying Mesozoic fault trends, lithological heterogeneities within the sedimentary package (Lonergan and Cartwright, in press) or can have a component oriented parallel to the general strike of the sedimentary layers. An orientation bias parallel to the strike of a slope is the most common and will exist at some stratigraphic interval on most datasets. The weak strike orientation biases found on any one map generally do not persist vertically from one faulted interval to the next within a single dataset and do not appear to exhibit regional consistency. Where the sedimentary packages dip and in particular have wedge-shaped depositional geometries, faults striking near-parallel to the strike of the sedimentary layers will preferentially dip up slope. This was noted by Higgs and McClay (1993), Clausen and Korstgård (1993) and Cartwright (1994a) on regional two-dimensional seismic data from the North Sea and has been confirmed by more detailed mapping on three-dimensional data-

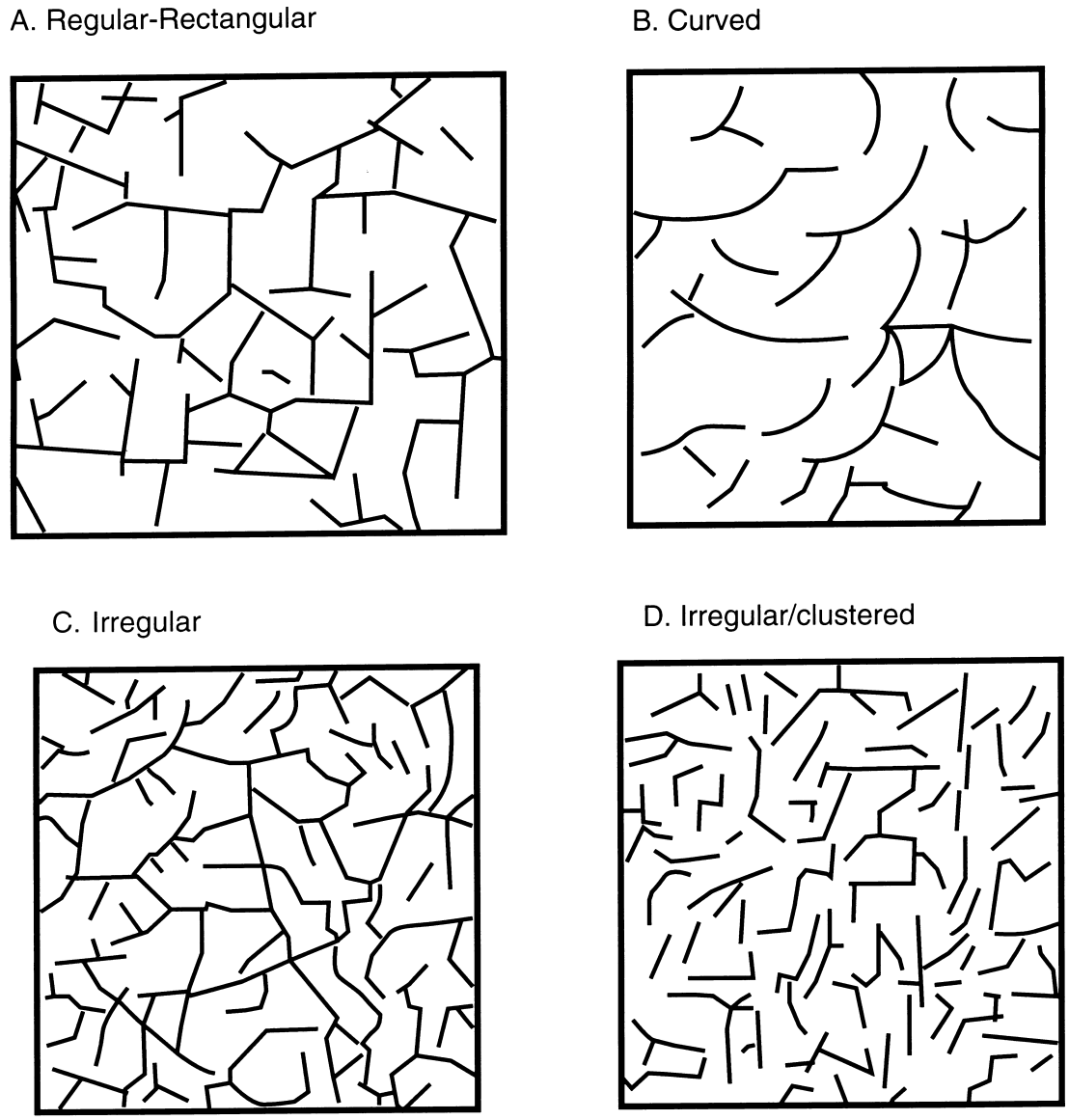

Fig. 3. Schematic end-member map patterns observed in polygonal fault datasets.

sets (Lonergan *et al.*, 1998; Lonergan and Cartwright, in press).

Fault trace lengths

Fault trace lengths for the polygonal fault maps typically range from under 100 m to 1000 m with a clustered distribution of fault trace lengths between 200–700 m (Fig. 5b) as the fault maps in Fig. 4 illustrate. All maps have fault length distributions with a rapid fall off in larger length faults and do not exhibit power-law length frequency distributions typical of other sorts of fault arrays. For example the curved map in Fig. 4(b), has longer faults than the other examples illustrated and the upper limit cut-off is about 1.8 km (Fig. 5b), but the irregular-connected map in Fig. 4(c) has shorter faults (a mean length of 311 m) and a cut-off at *ca.* 800 m (Fig. 5b). This upper limit in the fault length distributions is not due to sampling errors, as the sample area is several times larger than the maximum fault trace length on any map, but is a real feature of the data. An upper limit to fault trace length distributions is typical of cellular polygonal geometries that are scale dependent with a characteristic length scale (Korvin, 1992) and hence non-fractal. Joints also have regular non-fractal geometries (Gillespie *et al.*, 1993) suggesting that polygonal fault networks may have more similarities with joint populations, than with fault arrays of a tectonic origin which have been shown to have self-similarity in their size distributions over a range of scales (Scholz and Aviles, 1986; Hirata, 1989; Heffer and Bevan, 1990; Yielding *et al.*, 1992). All maps have a small percentage (generally less than 5%) of longer fault segments (>1 km) which mainly arise due to the linkage of shorter fault segments along the same trend. The

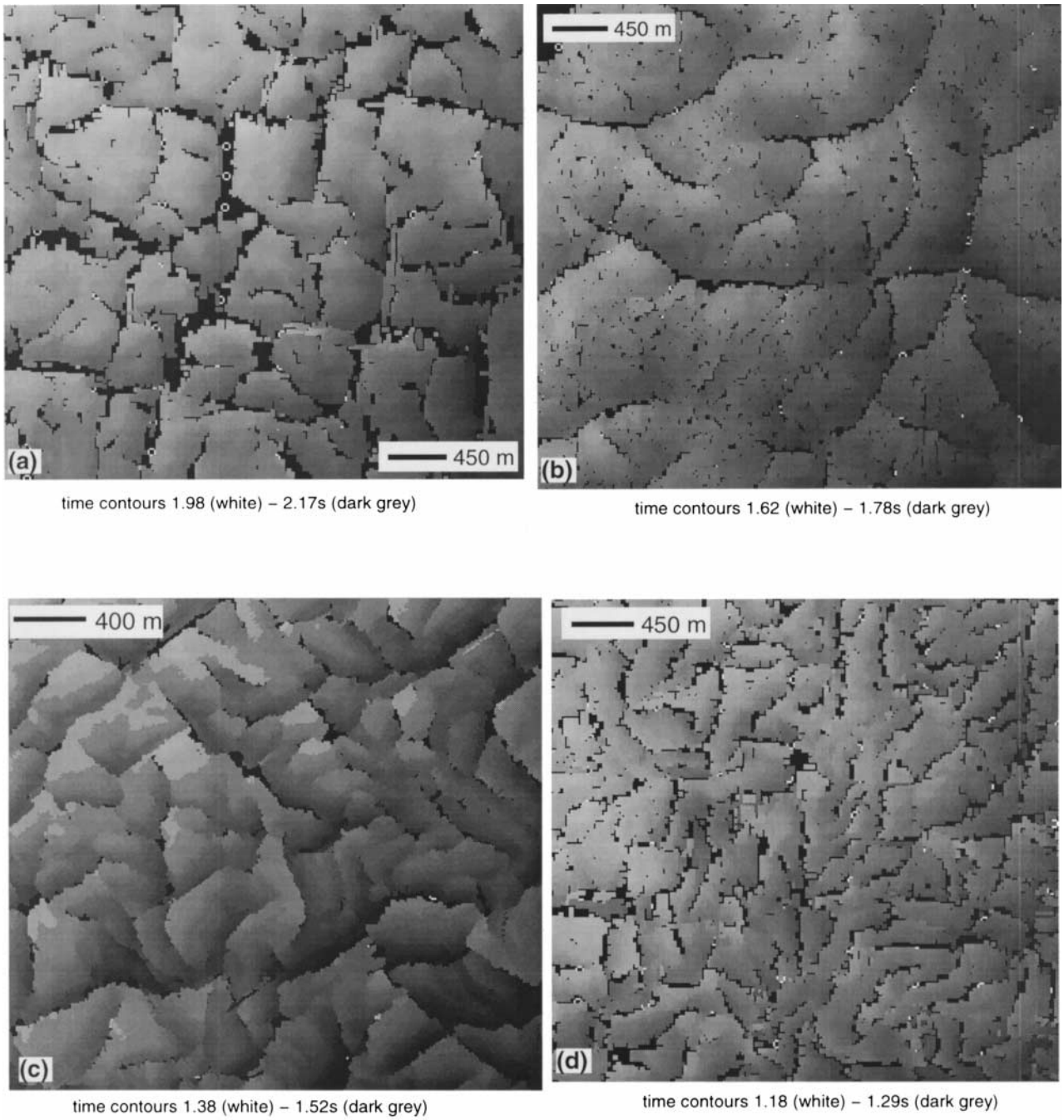

Fig. 4. Examples of end-member map patterns from two different seismic datasets in the central North Sea. Each map is a grey scale horizon time contour map. Black gaps in the horizon, or time contour, offsets represent horizon offsets (heave) due to faults. (a) Regular-rectangular map pattern, Eocene horizon; block 21-14; (b) Curved map pattern, Oligocene horizon; block 21-14. (c) Irregular map pattern, Oligocene horizon, block 16/26. (d) Irregular-clustered map pattern, lower Miocene horizon, block 21/14. All horizons dip very shallowly ($< 3^{\circ}$) from NW–SE.

truncation in all the fault trace length distributions of fault lengths less than 100 m is most likely due to the resolution limit of the map data. Line spacing is generally 25 m (more rarely 12.5 m) and thus short faults that that only occur on two lines (50 m length) are likely not to have been mapped.

There are variations in the individual fault length distributions. For example, the curved fault map has longer fault segments than the other maps and the two irregular fault maps have higher percentages of shorter faults between 100 and 200 m. Currently we do not have enough data to tell if these differences are systematic and typical of any one pattern type.

On one dataset from quadrant 30 of the central North Sea the primary polygonal pattern in one half of the dataset occurs at a scale larger than the other datasets, i.e. the mean lengths are between 1 and 2 km as opposed to 200–300 m (Fig. 6). By processing the autotracked horizon for dip and azimuth attributes a second set of shorter and smaller faults, close to the

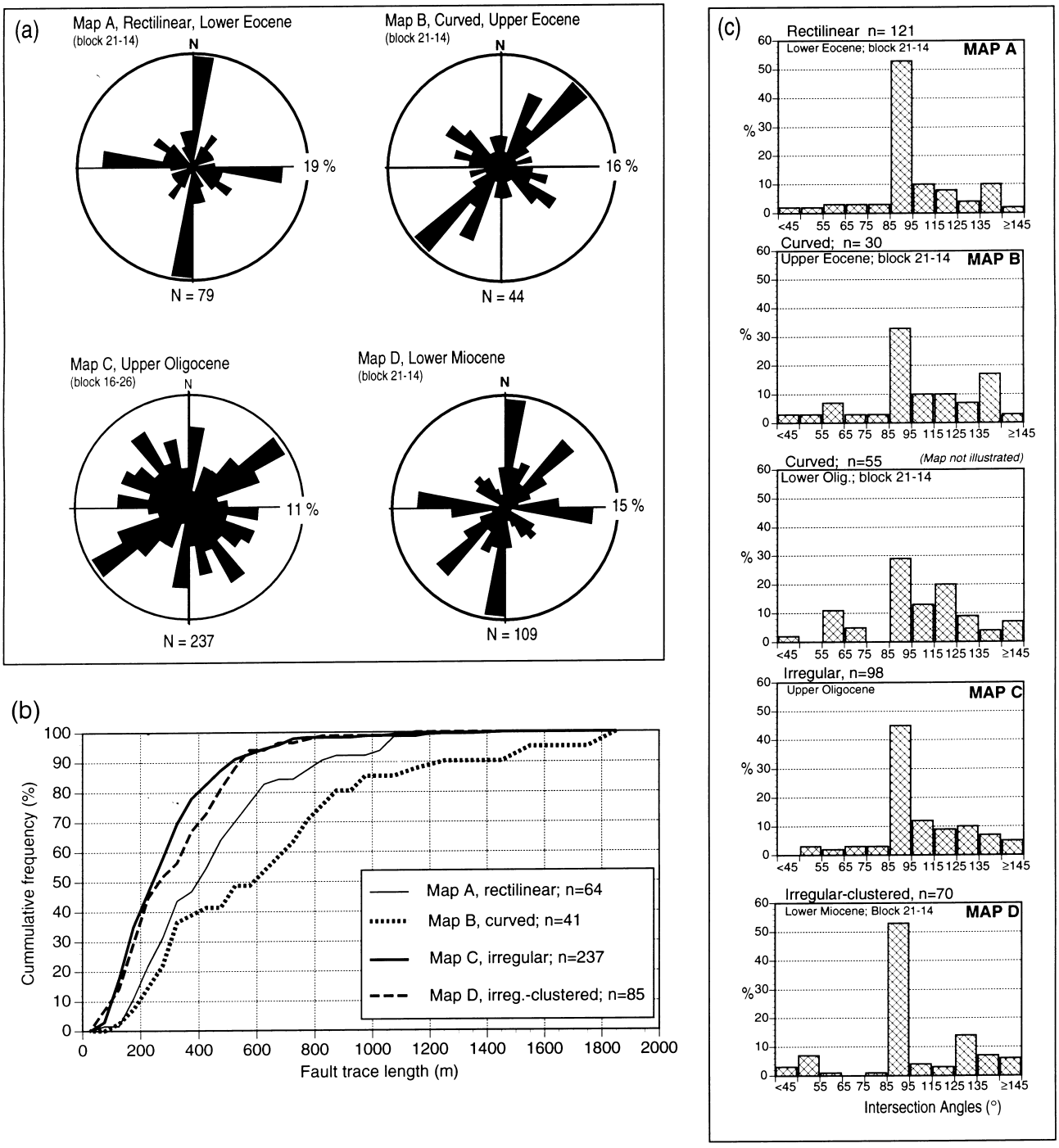

Fig. 5. Fault map statistics for maps illustrated in Fig. 4. (a) orientations; (b) fault trace lengths, cumulative frequency normalised to %; (c) intersection angles in plan view normalised to %.

data resolution limit within each 'polygon' was revealed (Fig. 6). These smaller faults intersect the larger-scale faults at 90°, generating a pattern similar to that sometimes observed in other materials undergoing volumetric contraction, where there are several generations of polygonal networks. For example Allen (1987) and Plummer and Gostin (1981) show examples of more than one generation of desiccation cracks forming on tidal flats, and Walker (1986) illustrates two generations of cracks in cornstarch. It thus appears that akin to other shrinkage phenomena there can be more than one generation of polygonal faults having successively smaller characteristic length scales. Although at any one scale, a polygonal geometry cannot be considered fractal because it is scale-bounded by the characteristic length scale of the polygon cells, when several generations of polygons form the resulting geometry can be fractal (Korvin, 1992). The evidence from this one dataset suggests that self-similar smaller-scale polygon faults or fractures formed within

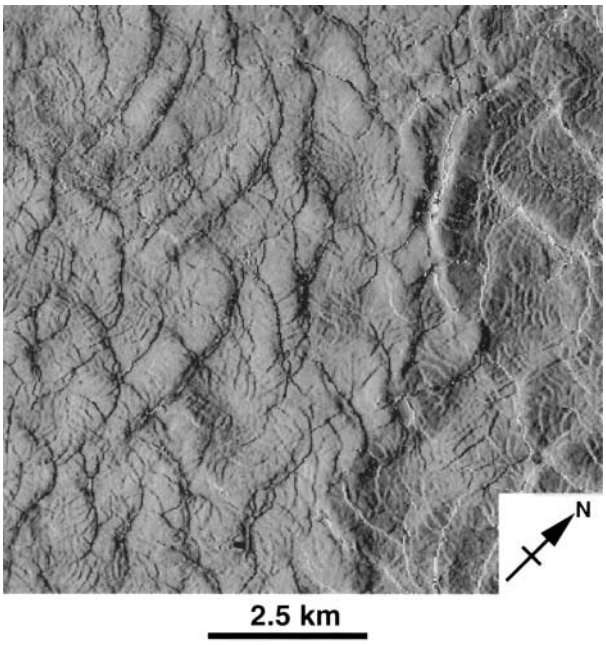

Fig. 6. Illuminated time-dip attribute map of an interpreted time-contour map, from a dataset in the southern central North Sea (Miocene horizon). The higher dips in darker grey or white, represent fault 'scarps'. Note the two sets of polygonal faults, with smaller faults within the polygons defined by the larger set of faults. The smaller faults tend to intersect the larger faults orthogonally. The artificial light illumination direction was from the east, hence westerly dipping faults are in shadow (dark grey); and easterly dipping faults are picked out in white. E–W trending faults are subdued.

the larger scale polygons may be a more ubiquitous feature of the North Sea mudrocks, but that so far our view of the polygonal geometry is constrained by the size of faults that can be resolved on three-dimensional seismic reflection datasets. Work by Verschuren (1992) describes outcrop examples of these faults in Eocene clays in Belgium with throws of several metres and reports of faults with polished surfaces and slickensides in core through the Paleocene and Eocene mudrocks in the North Sea (Conybeare, 1996, quadrant 22; Jaffri, 1993, quadrant 9) tends to support the suggestion that there may be several hierarchies of scale of polygonal faults developed in the North Sea Tertiary mudrocks.

Map intersection geometries

Measurements of fault segment intersection angles in plan view confirm that for all of the recognised fault pattern types, with the exception of the curved end-member map type, the majority of intersections are orthogonal (Fig. 5c). The curved map types have a broader spread of obtuse angles. On many maps we observe faults which curve rapidly in strike to form an orthogonal intersection with an adjoining linear fault trace segment. Similar observations have been made for a variety of different joint types (including desiccation cracks and ice-wedge polygons) (e.g. Lachenbruch, 1962; Pollard and Aydin, 1988). Pollard *et al.* (1982) attribute such patterns to the mechanical interaction of fractures where the stress field associated with one fracture can perturb the propagation direction of neighbouring fractures if the distance between them is small with respect to their dimensions. For simple tensile fractures a fracture propagating towards an existing fracture is deflected perpendicular to the maximum principal tensile stress (Lachenbruch, 1962; Pollard and Segall, 1987). Although the stress field for the dipping polygonal fault system is undoubtedly more complex than that of simple vertical tensile fractures, somewhat analogous mechanical interactions can be observed to have occurred.

Faults which terminate orthogonally against the convex side of a continuous fault (cf. the 'curved-T' intersections of de Graff and Aydin, 1987) are also observed. This pattern is attributed to high stresses on the convex side of the curved fracture (Lachenbruch, 1962). From the analysis of other structures formed in response to contraction such as mud cracks and columnar joints in lavas it has been observed that the abutting fracture can either propagate away from or toward the curved fracture (de Graff and Aydin, 1987; Aydin and de Graff, 1988).

The differences between predominantly orthogonal as opposed to non-orthogonal intersections have been noted in previous studies of polygonal and other regular repeat fracture patterns (such as joints) (Lachenbruch, 1962; Corte and Higashi, 1964; Allen, 1987; Pollard and Aydin, 1988 amongst others). In particular the difference between hexagonal patterns with predominantly three-way, approximately equiangular intersections, and orthogonal intersections have been discussed a number of times (Lachenbruch, 1962; Aydin and de Graff, 1988; Allen, 1987). Associated with this is the consideration of the implication of three-way intersections and whether or not their presence implies that the three fractures nucleated at a single point and propagated outwards. In polygonal systems that form due to contraction phenomena it seems that three-way 120° intersections arise in systems that contract rapidly, for example rapidly cooling lava flows and thin layered rapidly desiccating muds (Corte and Higashi, 1964; Grosiman and Kaplan, 1994). Lachenbruch (1962) has argued that many of the triple junctions that occur in more irregular polygonal networks may in fact not be true 'triple junctions' but arise from the evolution of a curved orthogonal (or T) intersection where orthogonal branching has occurred on the convex sides of bends too small to be detectable on open cracks. Work by Aydin and de Graff (1988) on columnar jointed lava flows would tend to support that conclusion. We have not mapped any polygonal fault arrays where the map pattern is dominated by three-way equiangular intersections, but three-way non-colinear intersections do occur as do non-orthogonal intersections where one fault terminates obliquely against a continuous fault. We cannot discount the

possibility that the non-orthogonal intersections are perhaps merely macroscopically non-orthogonal and at a small scale, close to the intersection, some of the obliquely abutting faults may indeed curve around to form orthogonal intersections.

Fault density

Another parameter that contributes to the variability in the fault polygon maps is the density of faulting. Most of the fault maps we have thus far examined have total fault trace lengths ranging from less than 1 km per square kilometre to over 4 km per square kilometre. The curved fault map in Fig. 4(b) falls at the lower end of that range with a mean of *ca*. 1.6 km of total fault length per km^2, where as the irregular fault map (Fig. 4c) with many closely spaced faults has a mean of more than 4 km of fault length per km^2. Maps with widely spaced, poorly connected fault networks tend to have the lowest fault densities.

Discussion of map patterns

The implications of the distinct geometries that are observed on maps are as yet unclear and are described and illustrated with the primary objective of giving an overview of the natural variability that is observed within this newly discovered fault system. We offer no conclusive explanations as to why some stratigraphic intervals or areas tend to have predominantly curved volumetric contraction faults as opposed to more regular, rectilinear faults, but it is likely to be affected by factors such as the slope on which the fault system develops, lithological variation (i.e. percentage clay fraction), degree of shrinkage, and the rate of shrinkage or fault formation. It is tempting to draw analogies with the sorts of patterns observed in naturally desiccating muds (Allen, 1987; Plummer and Gostin, 1981) or desiccation crack experiments (Corte and Higashi, 1964; Grosiman and Kaplan, 1994); for example, rapidly desiccating muds tend to form closely spaced short-sided cracks, whereas a more slowly desiccating thick-layered mud forms wider spaced rectangular/rectilinear cracks. Boundary effects and lithological heterogeneities also profoundly affect the patterns of desiccation cracks developed in muds.

THREE-DIMENSIONAL FAULT INTERSECTION GEOMETRIES

Although much information about the fault network can be extracted from an analysis of fault maps, each map is ultimately limited because it only represents a single two-dimensional slice through the three-dimensional geometry. Based on detailed mapping of 20–30 faults within two seismic datasets and the analyses of many maps and seismic sections, four main intersection types can be recognised that encompass most of the geometrical variability observed within the polygonal fault system. The fundamental difference to other non-polyphase deformation styles is that the faults strike in a wide variety of orientations. The resultant fault network consists of faults that abut or truncate against each other and link with each other in complex ways. An almost infinite variety of intersections between dipping planes can occur, but we restrict our discussion of intersection geometries to those that are observed most frequently within the polygonal fault system and those that mainly form branch lines as opposed to isolated branch points in three-dimensions. The spatial continuity or geometrical 'stability' of an intersection defines whether it occurs merely as a branch point or a branch line. The more fault segments there are forming an intersection, the more geometrical constraints there are on whether the intersection can persist as a line in space. Equally, because of geometrical constraints an intersection type can evolve from one type to another along a branch line. For all intersections, if the strike of a fault segment is defined, the orientation of a branch line in space will depend on the dip magnitude and direction of the faults forming the intersection. This is discussed further below, as relevant to the different intersection types. Under conditions of homogeneous strain, if there is synchronous motion on the fault segments joined at a branch line then the displacement direction (slip vector) on all faults must be parallel to the plunge of the branch line.

Fault intersection classes

The four main fault intersection types are illustrated schematically in Fig. 7, both in three-dimensions and in plan view (as they would appear on a map), and discussed with reference to the predominantly steeply plunging branch lines that form when faults with a wide range of strike orientations but similar dips intersect.

Class A. Two non-colinear faults which intersect at segment endpoints. The intersection angles are predominantly obtuse ($>90^\circ$) and the two faults making up the intersection both dip 'outwards' or 'inwards' with respect to their plan-view geometry (Figs 7 & 8a,b). It is geometrically feasible for one of the two fault segments to dip outwards and the other inwards (Fig. 8c), but no examples of such a geometry have been observed in the real datasets.

Class B. A principal fault and an adjoining fault which intersects the principal fault at any angle. For steeply plunging branch lines the principal fault will have two fault trace segments in plan view. Class B orthogonal intersections are similar to 'T' and curved-T intersections defined for joint sets (e.g. Pollard and Aydin, 1988 and references therein) except that the branch line is not required to plunge vertically.

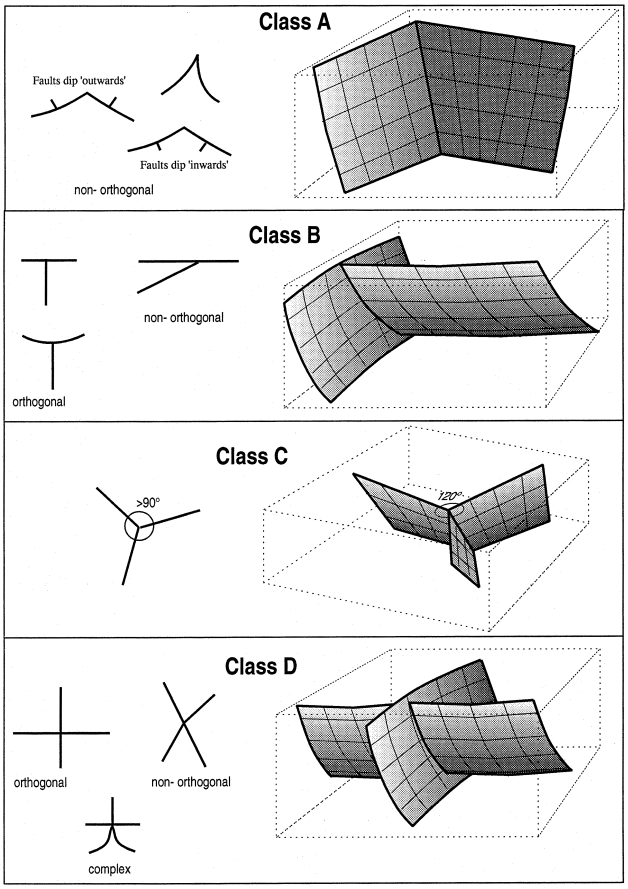

Fig. 7. Schematic diagram of main fault intersection types for the polygonal fault system.

Class C. Three non-colinear faults intersecting at a common branch line forming non-90° intersection angles. A Class C intersection can only form a continuous branch line instead of a branch point for a limited range of geometrical conditions. If the three faults are vertical then the branch line is geometrically stable and three planes can potentially remain connected along their entire vertical dimension [the Y intersections or triple junctions described in mudcracks (Corte and Higashi, 1964) and columnar jointed lava flows (de Graff and Aydin, 1987)]. If however the faults are distributed in an equiangular fashion, but the three planes dip, then it is more difficult for a geometrically stable branch line to form. If the three faults are labelled x, y and z, in an anticlockwise direction centred at the intersection point, and x dips towards y, y towards z and z towards x then the branch point cannot belong to a branch line unless the faults fold or form torqued shapes (Fig. 8d). If faults y and z dip 'towards' each other and have the *same* dip, then to form a continuous three-way intersection x must be a vertical fault (Fig. 8e). Lastly if one of z or y have a steeper dip then the other then the plunge of the z–y branchline geometrically constrains the direction in which x can dip to form a continuous three-way intersection (Fig. 8f). For Class C intersections only the geometry illustrated in Fig. 8(f) has been observed.

Class D. Four or more fault segments intersecting; the intersection can have four orthogonal angles, or one or more non-90° angles. For a four-way intersection to form a simple continuous branch line there are a restricted number of geometrical configurations possible. In the first instance if the Class D intersection is orthogonal, where the two segments of the same strike are x, x' and y, y', respectively then the only stable relationship where all four fault segments can remain connected is for x and x' to dip in the same direction, with the same dip magnitude and y–y' likewise (Fig. 8g). In a non-orthogonal case, for any prescribed strike the plunge of the branch line between any two of the four faults defines the dip magnitude and direction of the other two faults.

It may appear difficult to envisage how a Class A intersection forms. It seems most unlikely that the two faults segments propagated outwards from the intersection, implying initiation at a singularity, unless they initiate at an inhomogeneity or a flaw. However we note that all examples of Class A intersections have two fault segments that both dip 'outwards' or 'inwards' (Figs 7 & 8). It seems possible therefore that the two segments have grown towards each other and linked laterally to form a kinematically coherent fault that then acts as one structure. Acknowledging that the observed topologies of the fault surfaces and intersections are dependent on both the scale of the observations and the resolution limit at which the structure can be observed (e.g. Childs *et al.*, 1995; Pickering *et al.*, 1997) it is also feasible that beneath the resolution

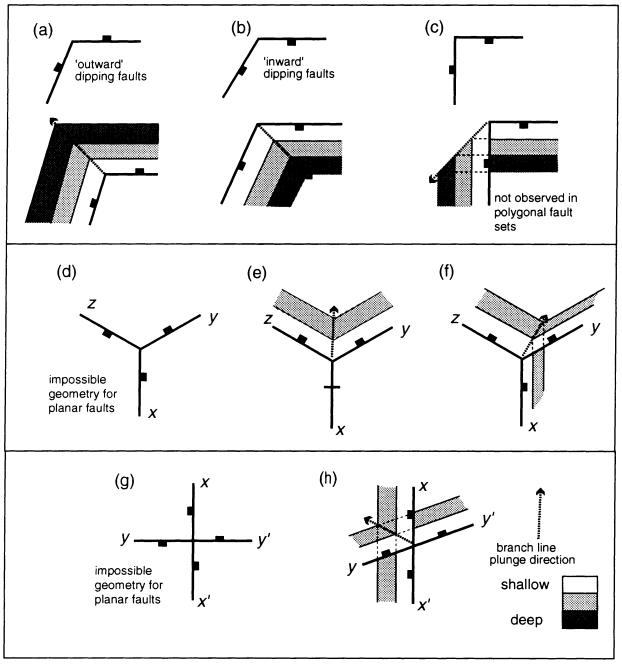

Fig. 8. Geometrical variations for selected intersection types. Diagrams are schematic fault plane contour maps (faults projected onto a map with structural contours). White–dark grey represents shallow–deep. Branch lines are shown with dashed lines; arrow is plunge direction. See text for further details.

limit of the seismic data one of the fault segments forming a Class A intersection does propagate out beyond the tip of the second fault segment forming a Class B intersection.

Class C intersections appear to be most widely developed as short branch lines or branch points. They are predominantly of the type illustrated in Fig. 8(f). No vertically plunging Class C branch lines have been identified to date. Another common geometry observed is a Class A branch line that evolves into a Class C intersection over a short interval of the branch line. It is also possible that Class C intersections arise as a form of modified B intersection where the principal fault is strongly curved, and at the resolution of our observations an orthogonal intersection cannot be identified between the principal and adjoining fault segments.

In the light of the geometrical possibilities discussed above we suggest that if faults are initially equally distributed in space and have an equal chance of growing

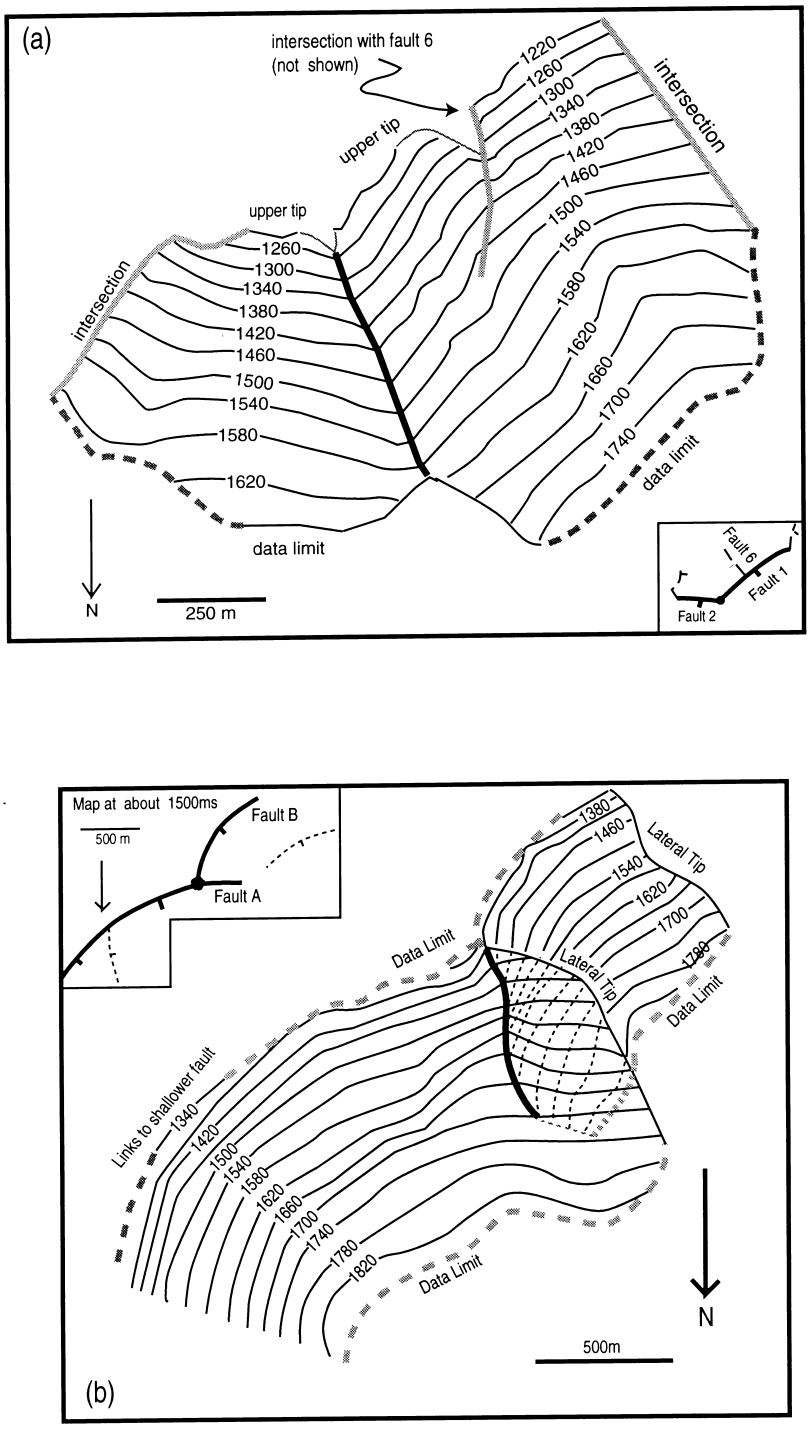

Fig. 9(a & b).

then Class B intersections are likely to be the most common. If any two faults at any orientation grow towards each other until they intersect they will form a B intersection when one intersects the other somewhere along its length. If two faults dipping in the same general direction, but with different strikes grow towards each other then their lateral tips might link forming an A intersection. Geometrically and kinematically three- or four-way intersections (Class C and D) are more constrained and hence are less likely to occur. In the absence of specific mechanical reasons favouring their formation, C and D type intersections might be expected to occur as branch points or short branch lines, with their occurrence being a function of fortuitous intersection of dipping planes growing to infill the volume. It is also possible that they arise due to sequential or later development of one or more of the fault segments forming the intersection.

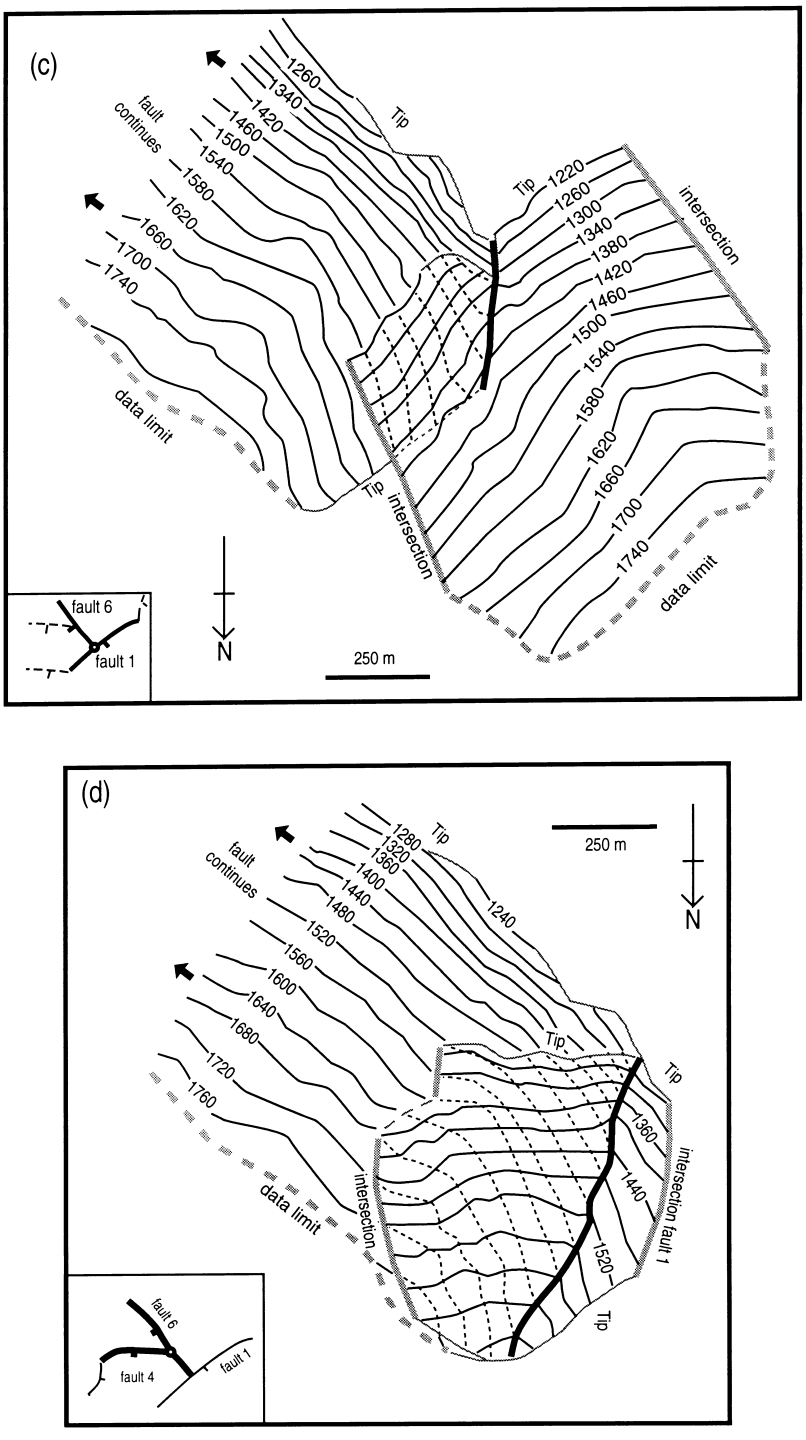

Fig. 9(c & d).

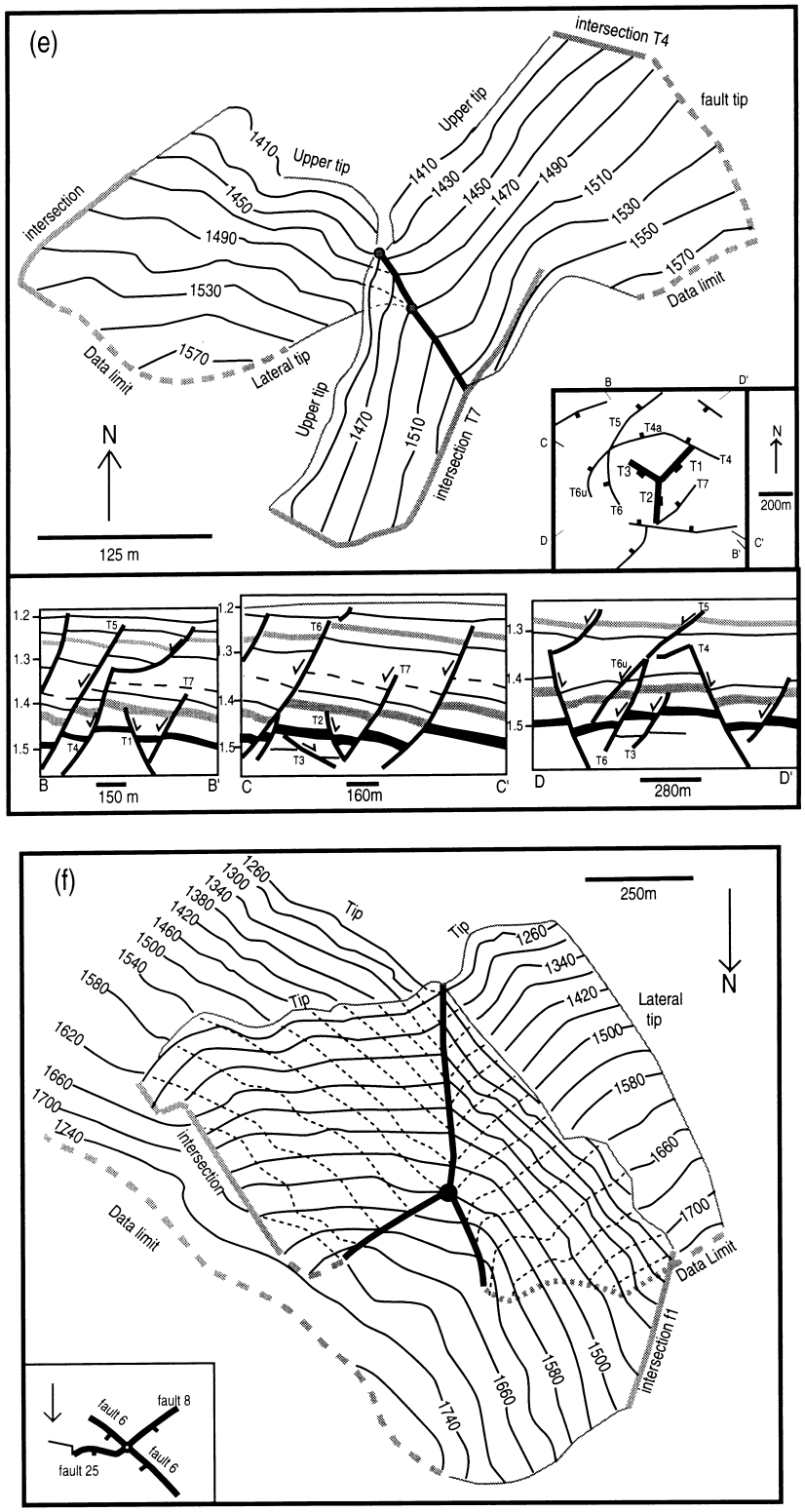

Fig. 9. Examples of the fault intersection types. Fault segments are shown as fault plane contour maps, contours in milliseconds two-way travel time, where lower values represent shallower times (and depths) beneath the seabed. The seismic velocity in the mapped interval shows little variation about a mean value of 2000 ms^{-1}, and the relative values can be approximately correlated with dimensions in metres (e.g. contour interval of 40 ms TWT ~40 m). The limits of the faults/fault segments are either shown as free tips, where the segment does not intersect another segment, or as an intersection (heavy black line). In the case of uncertainty due to lack of data resolution the fault limits are dashed and labelled data limit. Each diagram has an inset fault map showing the map relationship between intersecting and neighbouring faults (cf. Fig. 7). (a) Class A; (b) Class B orthogonal, curved faults; (c) Class B orthogonal, planar faults; (d) Class B, non-orthogonal; (e) Class C, three way intersection; Three cross-sections (line drawings from seismic data) illustrate the complex geometry of the faults in the vicinity of the Class C intersection; (f) Class D.

Examples of the polygonal fault intersection classes

Real examples of each of the intersection types are illustrated in Fig. 9. All the examples except one (Fig. 9b) come from a seismic survey in quadrant 16 of the central North Sea where the line and trace spacing is 12.5 m and the faults are well-imaged (Fig. 1). The group of faults occur from the shallowest faulted interval (Oligo-Miocene sediments), with clearly resolvable upper tips. There is more uncertainty associated with the interpretation of the lower limits of the faults because they extend into the lower-middle Oligocene low-amplitude interval (Lonergan and Cartwright, in press). Faults can be mapped with confidence through 400–500 m vertical thickness of the sequence. One of the Class B intersections comes from a dataset in quadrant 21 of the North Sea (Fig. 1a). In this case the line and trace spacing is 25 m and the two faults mapped come from the middle of the faulted interval (upper Eocene–lower Oligocene sediments). The upper limits of the two faults are poorly defined because they appear in part to link with faults developed shallower in the section and in part to truncate against overlying faults.

In each fault diagram in Fig. 9 the limits of the faults are either defined as a tip, if the fault does not intersect another fault, or as an intersection. In the case of uncertainty due to lack of data resolution the fault limits are dashed. The fault geometries are illustrated with fault plane contour maps, where the contours are in milliseconds two-way travel time (TWT).

A class A intersection is defined by two faults dipping to the NW (fault 1) and NNE (fault 2), respectively (Fig. 9a). The branch line which plunges NNW extends from 1260 ms to 1600 ms TWT. Beneath this point the two faults separate, and the larger fault (fault 1) extends 150 ms deeper. The lateral limits of both faults are defined by intersections with other faults. As a result, fault 2 has an upward tapering triangular geometry. The upper tip of fault 1 in particular is irregular and the tear occurs where fault 1 intersects two NW striking faults (not shown) close to its upper tip.

Three examples of Class B intersections are illustrated; two orthogonal intersections (Fig. 9b & c) and one non-orthogonal B (Fig. 9 d). The first of the B intersections forms between two curved faults where the smaller adjoining fault curves around to maintain an orthogonal intersection with the principal NW dipping fault. The branch line extends from 1380 ms to 1720 ms TWT and again both faults separate at greater depths. At the lower end of the faults, the larger fault extends furthest beyond the termination of the branch line. At the upper limit of the faults, away from the intersection point both faults extend 40 ms shallower and may even link with faults from an overlying tier. Although both faults have curved strikes they have planar cross-sectional profiles and are not listric. Only the larger fault shows a slight decrease of dip (or flattening) towards its lower limit. In contrast some other curved faults that have been mapped have gently listric profiles.

The second B intersection is formed by the intersection of NE (fault 1) and NW (fault 6) striking faults, where the NE striking fault forms the principal fault (Fig. 9c). Both faults extend from 1220 ms to at least 1740 ms TWT, but they only remain connected over a short distance (from 1220 ms to 1440 ms TWT) relative to the fault segment length in a dip direction. Note the irregular upper-tip of fault 6, a common feature of the upper tips of the shallowest fault set in this dataset, where they intersect with shallower fault segments of a different strike.

The non-orthogonal Class B branch line is formed by the intersection of the NW–SE striking fault 6 and an E–W fault, fault 4 (Fig. 9 d). The two faults dip synthetically, i.e. the principal fault (fault 6) dips towards rather than away from the adjoining fault. The branch line is the longest of any mapped and extends from 1280 to 1680 ms TWT, being continuous for the entire dip extent of fault 4. Of the fault intersections that have been mapped in detail very few have been found where the faults remain in contact over the entire dip-extent of one of the faults. Fault 4 has an irregular slightly triangular shape, tapering downward. The irregular eastern edge of the fault arises from intersections with two faults of differing strikes.

Class C intersections are not as common on maps as either Class B or A intersections and when maps are made at vertical intervals of greater than *ca.* 200 m Class C intersections are rarely traceable from one map level to a shallower or deeper one, implying that the branch lines are shorter than for the more common Class B and A intersections. In the example illustrated (Fig. 9e) the three-way branch line only extends for a depth of about 40 m from 1450 ms to 1490 ms. Beneath this point two of the faults remain connected (T1 and T2) forming a Class A intersection and the third fault (T3) separates. In comparison to the other faults mapped within this stratigraphic interval the three faults forming the three-way intersection are small, both in a strike and dip dimension. In the dip dimension they extend through a maximum of 200 m vertical thickness, whereas the majority of the faults in this interval extend for 400–500 m from the upper limit of the faulted interval at around 1200 ms TWT. The maximum fault trace lengths are also short (170 m for T2 and T3; 230 m for T1). The three faults forming the C intersection are located in the space between some larger faults (T4, T7, and T6, Fig. 9e) and each are bounded on their outer lateral edges by the surrounding larger faults which extend up to the upper limit of the faulted interval. T2 is constrained on three sides by intersections with other faults. It terminates against T7 at its lower edge forming a subhorizontal conjugate intersection. All three faults have free upper

tips and terminate at the same stratigraphic marker (see cross-sections in Fig. 9e).

A Class D branch line is formed by the intersection of the NW–SE striking fault 6 with a NE striking (fault 8) and E–W striking fault (fault 25) (Fig. 9f). The branch line extends from the upper tip of the faults at 1260 ms to a depth of 1540 ms TWT. Faults 8 and 25 remain connected to fault 6 beneath 1540 ms but the four-way branch line divides into two Class B branch lines to depths of 1640 and 1660 ms TWT, respectively. The split in the branch lines occurs where there is an inflection in fault 6. It is not clear whether the inflection in fault 6 caused the fault 8 and 25 branch lines 25 to diverge or whether the location of faults 8 and 25 influenced the propagation direction of fault 6 and caused it to bend. Both fault 8 and 6 extend beyond the termination of their branch line to a depth of about 1740 ms, but fault 25 is connected to fault 6 throughout its vertical extent. This is another example of an adjoining fault (fault 25) remaining in entire contact with a principal fault (i.e. fault 6) when the principal fault dips towards the adjoining fault. Fault 8 is somewhat unusual in that it has a free lateral tip along its entire dip-length on the opposite edge to the Class D–B intersection. Without further data it is impossible to say whether Class D intersections evolving into Class B intersections, either by two Bs joining or a D, splitting is a common characteristic of the polygonal fault networks.

FAULT SHAPES

The fault edges can be defined by free tips (relatively rare) or intersections with one or more faults. The faults can have a variety of shapes varying from crudely rectangular to triangular, curved-planar to curved-listric and irregular. Of the faults mapped thus far, the majority approximate to a rectangular shape with either subhorizontal long axes (e.g. fault 6, Fig. 9) or dip-parallel long axes (fault 8, Fig. 9f). Fault 2 (Fig. 9a) is a good example of a triangular tapering-upwards fault shape whose geometry is defined by the intersections with the adjoining faults. Faults A and B, (Fig. 9b) have curved map traces but have planar dips; other faults have curved map traces and listric cross-sections defining a more spoon-shaped geometry. Fault 4, (Fig. 9d) is a an example of an irregular shaped fault resulting from complex lateral intersections with three different faults. The majority of the faults studied come from the uppermost tier in the dataset and thus have predominantly free upper tips. The three faults making up the C-type intersection illustrated in Fig. 9(d) (faults T1, T2 and T3) terminate within the faulted interval and they too have free upper tips. A number of the faults (e.g. see faults 1 and 6 in particular) have irregular (even fronded) upper tips. All the faults mapped to date are partially intersecting, truncated or branching. Completely isolated, non-connected, faults are very rare.

If a stratigraphic unit containing polygonal fault deformation is mechanically decoupled from overlying or underlying layers, or there is just a single faulted interval in the volume, we expect there to be a majority of free upper and lower fault tips. But where there is a lot of overlap between polygonal fault sets from different faulted layers, linking or abutting upper and lower fault terminations are expected to predominate.

DISCUSSION

In the faults and intersections examined for this study we rarely observe faults remaining connected along their entire vertical (i.e. dip dimension) length. The longest branch lines relative to vertical fault dimension occur for class B intersections where the principal fault dips towards the adjoining fault and for class A intersections where the two faults have the same general dip direction (compare examples in Fig. 9). The lack of continuous branch lines suggests that intersections largely form because the faults propagate in all dimensions as displacement accrues and they abut against each other fairly randomly. If they nucleated at intersection points and propagated outwards from intersections they might be expected to remain connected, because they would be kinematically linked at the intersection. Hence it appears that the complex three-dimensional topologies are primarily a function of intersections between fault surfaces propagating in a wide variety of orientations and inclinations.

If faults are indeed intersecting in a near random fashion because of propagation in a wide range of directions then Class B intersections are likely to be those that occur most frequently, because they essentially only involve the intersection of two faults and the resultant intersection is topologically stable. In the group of faults that have been mapped in detail, Class B and A intersections are the most common and Class C and D intersections occur less frequently. Class C intersections tend to have much shorter branch lines than either A or B intersections and appear to occur where a third fault connects for a short distance with a longer A intersection. This could occur where three connected faults split into an A intersection and an isolated fault as they grow or alternatively the third fault joins the other two faults that are already linked in an A intersection. The mapped example of a type D intersection shows it splitting into two B intersections with increasing depth. This implies that the four-way branch line formed either by an initial four-way intersection splitting into two B intersections or by the merging of two B intersections.

The observations above have been made on a small area and mainly from one three-dimensional seismic

Table 1. Numbers of fault intersection classes present on maps from datasets in quadrant 21 and 16 (expressed as % of total number of intersections, *n*). Data for Class B intersections are subdivided into orthogonal and non-orthogonal intersections. Maps A–D are illustrated in Fig. 4

Map	A (mainly > 90°)	B (totals)	***B*** ***(2–3, 90°)***	***B*** ***(2–3, ≠90°)***	C (three way)	D (4, 90°)	D (4, > 4, non-90°)	totals	***n***
Upper Eocene (block 21/14) MAP B;	42%	53%	*32%*	*21%*	5%	—	—	100%	19
Lower Olig. (block 21/14) MAP C;	31%	52%	*24%*	*28%*	14%	—	3%	100%	29
Oligocene (block 16–26)	33%	43%	*27%*	*16%*	14%	8%	2%	100%	49
Lower Miocene (block 16/26) MAP A;	19%	65%	*47%*	*19%*	9%	7%	—	100%	43
Lower Eoc. (block 21/14) MAP D;	21%	61%	*40%*	21%	13%	3%	1%	100%	67
Miocene (block 21/14)	39%	56%	*39%*	*17%*	5%	—	—	100%	41

dataset, although similar relationships have been seen on the other datasets. To consider how representative the conclusions on frequency of occurrence of any one intersection type might be for polygonal fault systems in general, a number of maps, including those illustrated in Fig. 4, have been studied in detail. Although maps are limited in that they do not provide any information about how continuous or otherwise an intersection type might be and any horizontal branch lines will tend to be under-represented they are still useful in that they enable us to rapidly assess which intersection types are most common in the polygonal fault arrays over a wide area in the North Sea. On some datasets it is not possible to map fault surfaces because of zones of poor data resolution (low seismic amplitudes/lack of continuous reflections) between mappable horizons and thus fault maps provide us with our only useful intersection data. On the maps studied, making up a total area of 216 km^2, Class B intersections make up over 50% of all intersection types on the maps (Table 1), which concurs with the predictions and observations already discussed. Class A intersections are the next most common making up 20–40% of the total number of intersections at one map level. Class C

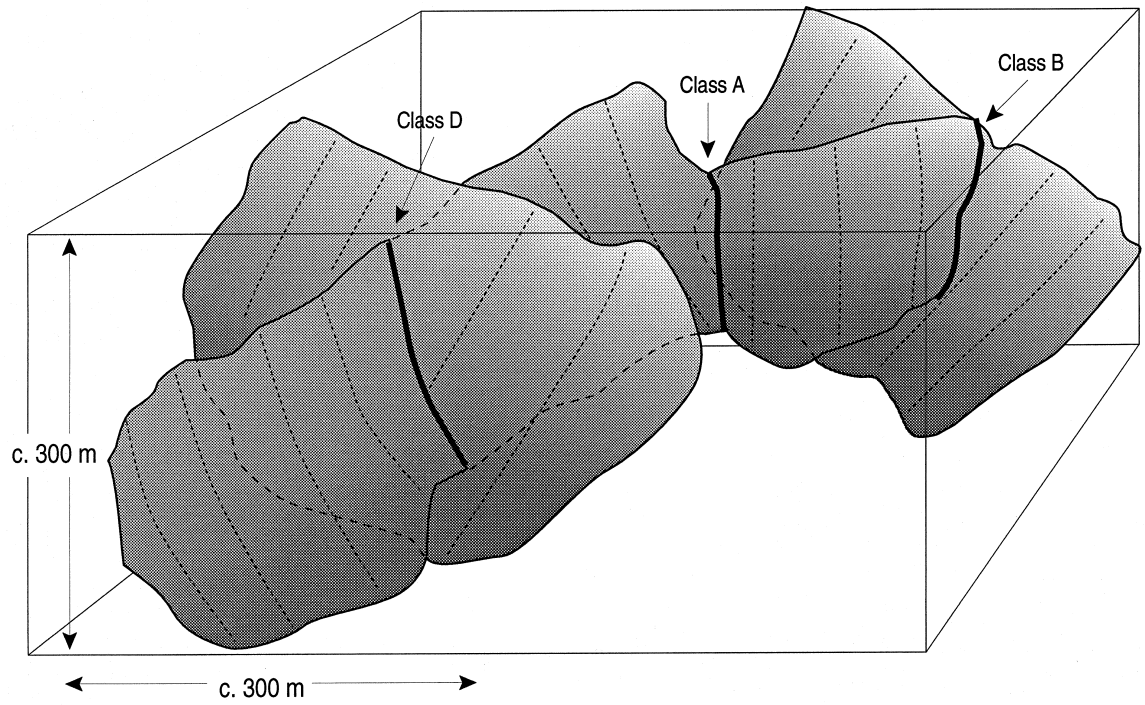

Fig. 10. Summary diagram illustrating different fault segments interlinked to form polygons with three of the intersection types defined in the text. Smaller faults (not shown) with other and similar intersection geometries typically infill the intervening volumes between the larger faults illustrated.

intersections only form between 5 and 14% of the intersections at any one map level. Class D intersections with steeply plunging branch lines are rare (< 5%). It is difficult to assess whether Class D intersections might be more common if conjugate horizontal/subhorizontal branch lines were to be sampled more fairly. Subhorizontal branch lines in the form of splays and conjugates are observed when fault surfaces are mapped but our studies so far suggest that they are much less common than steeper branch lines. Not all sub-horizontal branch lines are missed on maps; if gently plunging they will form acute A, B or D intersections.

The previous section has established the main components of the three-dimensional geometry of the polygonal fault arrays by investigating the variety of intersection relationships between adjoining fault segments. In the volume all the faults appear to interact and at one end of a segment a fault may form a two-way Class A intersection while its other lateral extent may be part of a B or D intersection. Similarly a lateral edge of a fault may form two different intersection types. Figure 10 illustrates schematically how these individual intersection types link up to form the three-dimensional polygonal networks. This diagram shows a number of intersecting faults that fill most of the vertical extent of the volume. However smaller faults (such as the Class C intersection illustrated in Fig. 9e) infill the intervening areas and may terminate by truncating against larger adjacent faults. With such a complex space-filling geometry it becomes clear how maps, made by slicing a three-dimensional geometry at different vertical levels, may look quite different even if made within a single stratigraphic tier.

CONCLUSIONS

The polygonal fault arrays developed in Lower Tertiary mudrocks in the North Sea exhibit a variety of different map styles all of which are broadly polygonal but in detail include regular-rectilinear, curved and irregular-random polygonal patterns. All maps have certain features in common. Particularly they all have fault traces distributed in a wide variety of orientations, and exhibit a predominance of orthogonal fault segment intersection angles. Fault trace length distributions have an upper limit which is a characteristic of this fault system and fundamentally different to the scale invariant length distributions of tectonic faults.

In three-dimensions the fault segments form four main intersection types. These intersection types have been defined according to the number of faults forming the intersection and the angular relationships at the intersection. Two faults intersecting at their ends are defined as a Class A intersection whereas two faults intersecting along the length of the 'principal' fault is defined as a Class B intersection. Three non-colinear faults intersecting define a Class C intersection and Class D intersections are formed where four or more segments intersect.

The three-dimensional geometry appears to result from the intersections of a volume filling fault array, where faults have propagated in all directions as they grew. Slicing the resultant complex topology at different horizontal levels generates maps with different fault patterns.

Our results have better defined the complex geometries of the intersecting polygonal fault systems deforming North Sea mudrocks. We believe that this geometrical description is the first step in understanding how these faults may be growing. Further work based on displacement analysis using this geometrical framework will provide more valuable insights into the mode of formation and growth of polygonal fault networks.

Acknowledgements—Fina Exploration U.K. are thanked for financial support and we acknowledge Fina and their partners for permission to publish seismic data from blocks 16/26 and 21/14 in the North Sea. LL is funded by the Royal Society and RJ by a NERC ROPA grant. We are also grateful to Schlumberger-Geoquest for generous technical support with the CHARISMA seismic interpretation package. Thanks to Chris Mansfield, Edwin Tervoort and Dustin Lister for helpful discussions; and to journal reviewers C. Dart, H. Fossen and J. P. Evans for useful comments.

REFERENCES

Allen, J. R. (1987) Desiccation of mud in the temperate intertidal zone: studies from the Severn Estuary and eastern England. *Philosophical Transactions of the Royal Society of London* **B. 315,** 127–156.

Aydin, A. and de Graff, J. M. (1988) Evolution of polygonal fracture patterns in lava flows. *Science* **239,** 471–476.

Bahorich, M. and Farmer, S. (1995) 3-D seismic discontinuity for faults and stratigraphic features: the coherence cube. *The Leading Edge* **14,** 1053–1058.

Barnett, J. A. M., Mortimer, J., Rippon, J. H., Walsh, J. J. and Watterson, J. (1987) Displacement geometry in the volume containing a single normal fault. *American Association of Petroleum Geologists Bulletin* **71,** 925–937.

Cartwright, J. A. (1994a) Episodic basin-wide fluid expulsion from geopressured shale sequence in the North Sea basin. *Geology* **22,** 447–450.

Cartwright, J. A. (1994b) Episodic basin-wide hydrofracturing of overpressured Early Cenozoic mudrock sequences in the North Sea Basin. *Marine and Petroleum Geology* **11,** 587–607.

Cartwright, J. A. (1996) Polygonal fault systems: A new type of fault structure revealed by 3D seismic data from the North Sea Basin. In *Applications of 3-D seismic data to exploration and production*, eds P. Weimer and T. L. Davis, pp. 225–230. American Association of Petroleum Geologists studies in Geology no 42. and SEG Geophysical developments Series no 5.

Cartwright, J. A. and Lonergan, L. (1996) Volumetric contraction during the compaction of mudrocks: a mechanism for the development of regional-scale polygonal fault systems. *Basin Research* **8,** 183–193.

Cartwright, J. A., Trudgill, B. D. and Mansfield, C. S. (1995) Fault growth by segment linkage: an explanation for scatter in maximum displacement and trace length data from the Canyonlands Grabens of SE Utah. *Journal of Structural Geology* **17,** 1319–1326.

Cartwright, J. and Lonergan, L. (1997) Seismic expression of layer-bound fault systems of the Eromanga and North Sea Basins. *Exploration Geophysics* **28,** 323–331.

Cartwright, J. and Dewhurst, D. (1992) Global distribution of layer-bound compaction faults. *Geological Society of America Bulletin* (in press).

Childs, C., Watterson, J. and Walsh, J. J. (1995) Fault overlap zones within developing normal fault systems. *Journal of the Geological Society of London* **152,** 535–549.

Clausen, O. R. and Korstgård, J. A. (1993) Small scale faulting as an indicator of deformation mechanism in the Tertiary sediments of the northern Danish Central Trough. *Journal of Structural Geology* **15,** 1343–1358.

Conybeare, D. M. (1996) Diagenesis and reservoir quality in the Everest Complex, North Sea. PhD thesis, University of London (Imperial College).

Corte, A. E. and Higashi, A. (1964) *Experimental research on desiccation cracks in soil*, pp. 1–76. Research Report—Corps of Engineers, U. S. Army, Cold Regions Research and Engineering Laboratory.

Cowie, P. A., Vanneste, C. and Sornette, D. (1993) Statistical physics model for the spatiotemporal evolution of faults. *Journal of Geophysical Research* **98,** 21809–21821.

Dalley, R. M., Gevers, E. C. A., Stampfli, G. M., Davies, D. J., Gastaldi, C. N., Ruitenberg, P. A. and Vermeer, G. J. O. (1989) Dip and azimuth displays for 3D seismic interpretation. *First Break* **7,** 87–95.

Dawers, N. H., Anders, M. H. and Scholz, C. H. (1993) Growth of normal faults: displacement–length scaling. *Geology* **21,** 1107–1110.

de Graff, J. M. and Aydin, A. (1987) Surface morphology of columnar joints and its significance to mechanics and direction of joint growth. *Geological Society of America Bulletin* **99,** 605–617.

Diegal, F. A. (1986) Topological constraints on imbricate thrust networks, examples from the Mountain City window, Tennessee, U.S.A. *Journal of Structural Geology* **8,** 269–279.

Gillespie, P. A., Walsh, J. J. and Watterson, J. (1992) Limitations of dimension and displacement data from single faults and the consequences for data analysis and interpretation. *Journal of Structural Geology* **14,** 1157–1172.

Gillespie, P. A., Howard, C. B., Walsh, J. J. and Watterson, J. (1993) Measurement and characterisation of spatial distributions of fractures. *Tectonophysics* **226,** 113–141.

Grosiman, A. and Kaplan, E. (1994) An experimental study of cracking induced by desiccation. *Europhysics Letters* **25,** 415–420.

Heffer, K. J. and Bevan, T. G. (1990) Scaling relationships in natural fractures: Data Theory and Application. *Society of Petroleum Engineers*, **20981**, Euopec 90, The Hague, 367–375..

Higgs, W. G. and McClay, K. R. (1993) Analogue sandbox modelling of Miocene extensional faulting in the Outer Moray Firth. In *Tectonics and Seismic Sequence Stratigraphy*, ed. G. D. Williams and A. Dobb, pp. 141–162. Geological Society Special Publication, **71**.

Hirata, T. (1989) Fractal dimension of fault systems in Japan; fractal structure in rock fracture geometry at various scales. *Pure and Applied Geophysics* **131,** 157–170.

Hoetz, H. L. J. G. and Watters, D. G. (1992) Seismic attribute mapping for the Annerveen Gasfield, The Netherlands. *First Break* **10** (2), 41–51.

Jaffri, F. (1993) Cross-cutting sand bodies of the Tertiary. Beryl Embayment, North Sea. PhD thesis, University of London.

Kindle, E. M. (1917) Some factors affecting the development of mud cracks. *Journal of Geology* **25,** 135–144.

Korvin, G. (1992) *Fractal models in the Earth Sciences*. Elsevier Science Ltd, Oxford, Amsterdam, London.

Lachenbruch, A. H. (1962) Mechanics of thermal contraction cracks and ice-wedge polygons in permafrost. *Geological Society of Americal Special Paper* **70,** 69.

Lonergan, L., Cartwright, J., Laver, R. and Staffurth, J. (1998) Polygonal faulting in the Tertiary of the Central North Sea—Implications for reservoir geology. In *Structural Geology in Reservoir Characterisation*, eds M. P. Coward, S. Daltaban and H. J. Johnson. Geological Society Special Publication **127**, 191–207.

Lonergan, L. and Cartwright, J. (1998) Polygonal shrinkage faults and their influence on reservoir geometries in the Alba Field, U.K. Central North Sea. *American Association of Petroleum Geologists Bulletin* (in press).

Neal, J. T., Langer, A. M. and Kerr, P. F. (1968) Giant desiccation polygons of Great Basin Playas. *Geological Society of America Bulletin* **79,** 69–90.

Oldham, A. C. and Gibbins, N. M. (1995) Lake Hope 3D—A case study. *Exploration Geophysics* **26,** 383–394.

Peacock, D. C. P. and Sanderson, D. J. (1991) Displacements, segment linkage and relay ramps in normal fault zones. *Journal of Structural Geology* **13,** 721–733.

Pickering, G., Peacock, D. C. P., Sanderson, D. J. and Bull, J. M. (1997) Modeling tip zones to predict the throw and length characteristics of faults. *American Association of Petroleum Geeologists Bulletin* **81,** 82–99.

Pollard, D. D., Segall, P. and Delaney, P. T. (1982) Formation and interpretation of dilatant echelon cracks. *Geological Society of America Bulletin* **93,** 1291–1303.

Pollard, D. D. and Aydin, A. (1988) Progress in understanding jointing over the past century. *Geological Society of America Bulletin* **100,** 1181–1204.

Pollard, D. D. and Segall, P. (1987) Theoretical displacements and stresses near fractures in rock: with application to faults, joints, veins dikes and solution surfaces. In *Fracture Mechanics of Rocks*, ed. B. K. Atkinson, pp. 277–349. Academic Press, London.

Plummer, P. S. and Gostin, V. A. (1981) Shrinkage cracks: desiccation or synaeresis? *Journal of Sedimentary Petrology* **51,** 1147–1156.

Scholz, C. H. and Aviles, C. A. (1986) The fractal geometry of faults and faulting. In *Earthquake source mechanics*, eds S. Das, J. Boatwright and C. H. Scholz, pp. 147–155. Geophysical Monograph. American Geophysical Union. Washington DC, U.S.A., **37**.

Sheriff, R. E. (1977) Limitations on resolution of seismic reflections and geologic detail derivable from them. In *Seismic stratigraphy; applications to hydrocarbon exploration*, ed. C. E. Payton, pp. 3–14. Memoir **26**, American Association of Petroleum Geologists, Tulsa, USA.

Verschuren, M. (1992) An integrated 3D approach to clay tectonic deformation. PhD Thesis. Universiteit Gent.

Walker, J. (1986) Cracks in a surface look intricately random but actually develop rather systematically. *Scientific American* **25,** 178–186.

Willemse, E. J. M. (1997) Segmented normal faults: Correspondence between three-dimensional mechanical models and field data. *Journal of Geophysical Research* **102,** 675–682.

Yielding, G., Walsh, J. and Watterson, J. (1992) The prediction of small-scale faulting in reservoirs. *First Break* **10,** 449–460.